Supporting Information

Near-Field Infrared Pump-Probe Imaging of Surface Phonon Coupling in Boron Nitride Nanotubes

*Leonid Gilburd,[1] Xiaoji G. Xu,[1,2] Yoshio Bando,[3] Dmitri Golberg,[3] and Gilbert C. Walker[1]**

[1]Department of Chemistry, University of Toronto, Toronto, Ontario, M5S 3H6, Canada

[2] Department of Chemistry, Lehigh University, 6 East Packer Avenue Bethlehem, Pennsylvania 18015, United States

[3]National Institute for Materials Science (NIMS), Tsukuba, Ibaraki 305-0044, Japan

Email: gwalker@chem.utoronto.ca

Spectral analysis – tapered tube – with vs without pump field

Relative absorption spectra from different locations along the tube are presented in Figure S1. The spectra were normalized by the laser output intensity. In order to investigate whether heating is the main mechanism producing the observed spectra two probe spectra from each location are presented – with (solid colored line) and without (black dashed line) the presence of the pump field. The comparison indicated that having the additional field (which causes additional heating) does not significantly affect the absorption spectra of the tube. Thus, we conclude that heating is not the main coupling mechanism.

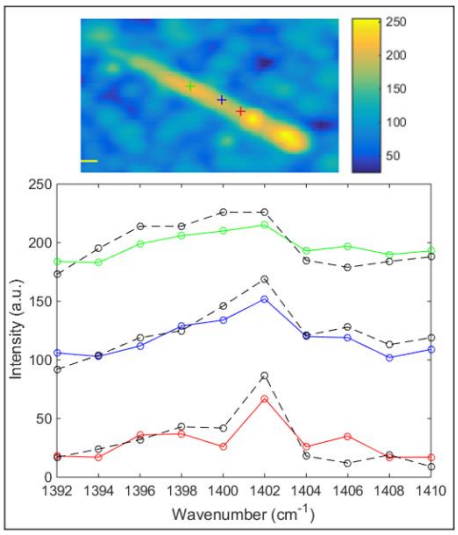

Figure S1. Spectra at 3 different locations along the tube (scattered probe field measured in the presence of the pump field). At each location a spectrum without the pump field (black dash line) is shown.

Spectral analysis – double tube – SPhP influence

The spectrum in Figure S2.a is very similar to the tapered tube (Figure S1). The double tube clearly show the presence of the SPhP standing wave on the left side of the tube (please refer to the paper). The spectrum from 3 different locations, where the SPhP standing wave is supported, is presented on Figure S2.b. The comparison of the absorption spectrum shows how the presence of the SPhP standing wave affects the spectral response.

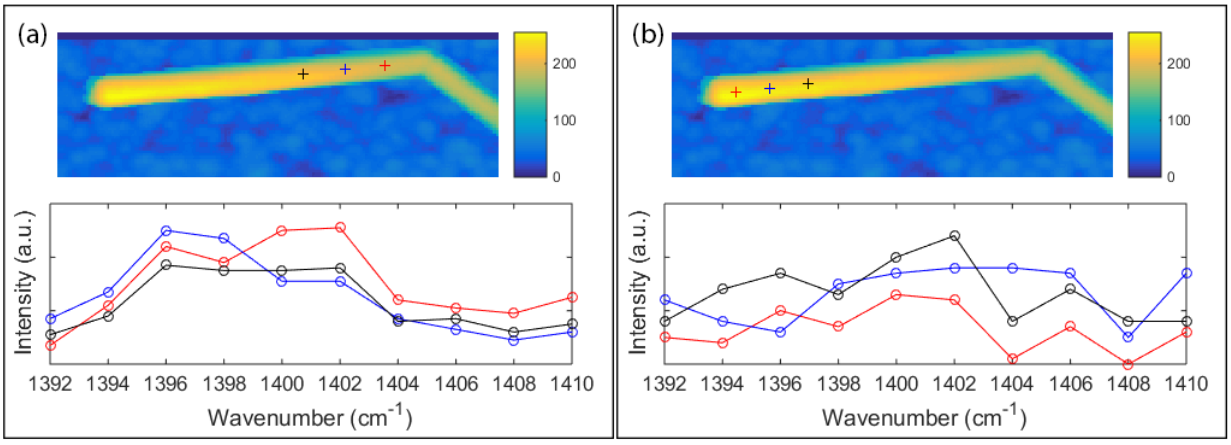

Figure S2. Spectrum from the double tube. (a) Consistently featured spectra from 3 different locations on the right side of the tube. (b) Broad, less-featured spectra from different locations along the left side of the tube, where the SPhP standing wave is dominant.

Pump/probe – On/Off

The series of images in Figure S3 were collected in presence/absence of the pump/probe fields. It shows that without the pump field, the side band image shows only noise (Figure S33.d). No signal on the side band images was detected when the pump field was present, but the probe field was turned off. This proves that the pump-induced signal was demodulated from the probe signal.

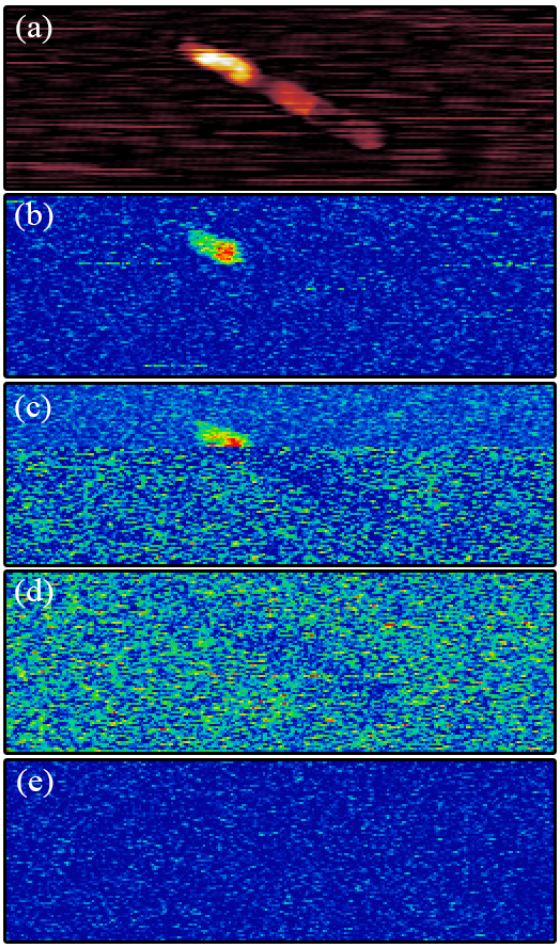

Figure S3. Near field images. a) Out-of-phase (imaginary) response of the tapered tube at 1408 cm^{-1} and (b) the corresponding pump-induced (at 1532cm^{-1}) excitation. (c) The following scan, during which the pump laser was turned off. Sideband image with pump laser is being turned off (d) and on (e) but without the probe laser.

A TEM study of BNNTs from the same batch

We studied more than 50 different tubes from the same batch, using a TEM (Hitachi H-7000) at 75 and 100 kV at different magnifications. About 10% of the tubes were cylindrical tubes without any major defects. Black spots in the image (see Figure S.a) are caused by the orientation of the BN layers parallel to the incident electron beam[1], 40% of the tubes were polygonal tubes that showed almost equal separation between the black dots. The remaining tubes showed a disordered arrangement of the black dots either along the whole tube or in part of it (see Figure S.b). In about 80% of all tubes structural defects were found in the inner part, while the outer diameter is unchanged. A few representative defects are shown on Figure S.c-f. Those defects would be undetectable in a standard tapping mode AFM topography scan, which was used in our experiment. The structural defects are often accompanied by some sp^3 hybridization which can cause mode shifting[2] and possibly the phonon mode coupling.

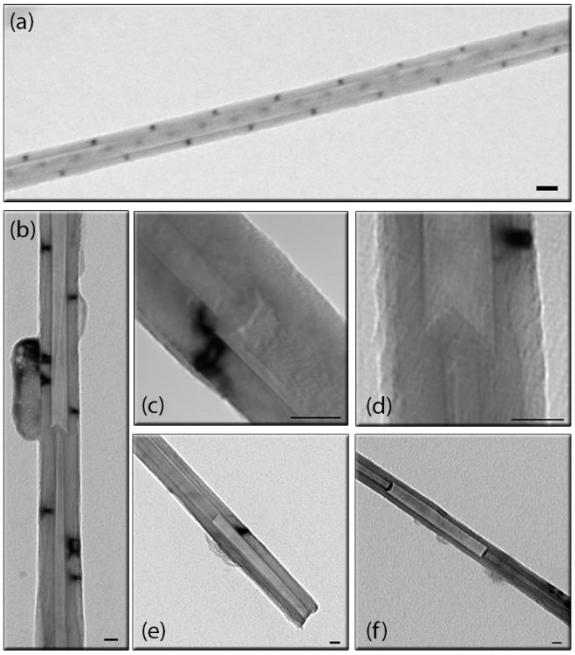

Figure S4. TEM images of different defects in BNNTs. Scale bar is 20 nm.

Polarization rotation by PEM

The polarization rotation was achieved using a photo-elastic modulator[3] (PEM 90, Hinds Instruments) operating at 'half wavelength' mode. A schematic presentation of the polarization state is provided in Figure S5. The light source is polarized in the direction parallel to the AFM tip. The PEM was mounted 45 degrees to the horizontal direction, such that the incident pump laser light polarization is equivalent to 'zero' retardation on the graph. In such configuration, the incident to the AFM tip polarization changes from parallel to perpendicular. This creates a polarization beating on the tip without changing the optical pressure. Sequentially, the near field changes the polarization. This causes beating in the excitation polarization.

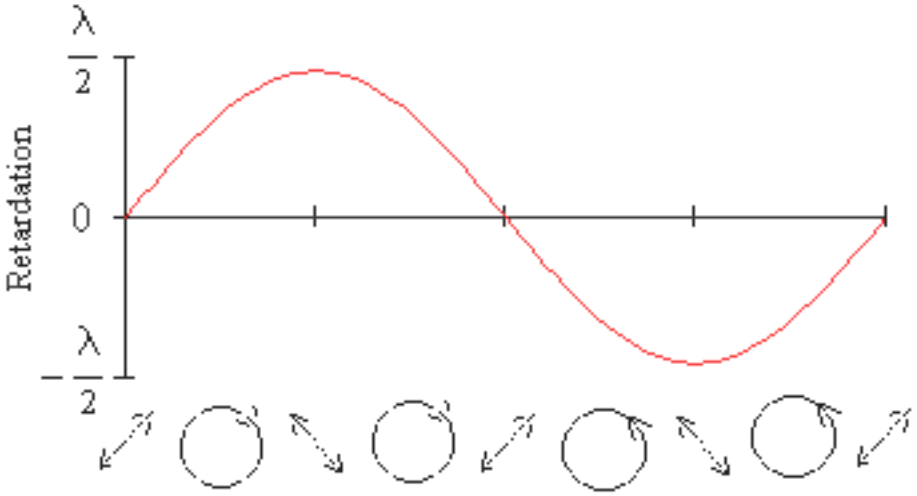

Figure S5. Light output polarization during a full PEM cycle in the 2Ω' regime.

Theory of the Signal

The near-field scattering from a sharp metallic tip in the proximity of a dielectric sample can be theoretically described by the image dipole model[4,5,6,7] (see Figure S6.a). The sharp tip apex acts as a dipole with a polarizability determined by its material dielectric function and tip radius. The polarizability of the dipole is determined by Eq. (S1).

$$\alpha = 4\epsilon\pi r^3 \frac{\epsilon_t - 1}{\epsilon_t + 2} \qquad (S1)$$

where ϵ_0 is the vacuum permittivity, ϵ_t is the relative dielectric function of the tip material, and r is the radius of the tip, typically in the range of 10 to 20 nm, depending on fabrication processes. The tip is typically coated with a noble metal: gold, silver or platinum, with minimum absorption at mid infrared frequencies. In the linear image dipole model, in the presence of *one* electric field (ω), the induced polarization of the tip is expressed by $P(\omega) = \alpha E(\omega)$, where $E(\omega)$ is the local electric field at the tip dipole location. If the tip apex is at a distance d from the sample surface, the electric field at the surface from the induced dipole is $P(\omega)/2\pi(d + r)^3$. Such an electric field generates a polarization in the dielectric sample. The field produced by the generated charge distribution is given by an image dipole inside the sample, at an equal distance d from the sample surface (see Figure 1a). The image dipole has the polarization of $\beta(\omega)P(\omega)$. $\beta(\omega) = (\epsilon(\omega) - 1)/\epsilon(\omega) + 1)$, the coefficient that satisfies the boundary conditions of Maxwell equations at the sample surface.

The dielectric function $\epsilon(\omega)$ is related to the sample susceptibility $\chi(\omega)$ through $\epsilon(\omega) = 1 + \chi(\omega)$. $\beta(\omega)$ can also be written as $\beta(\omega) = \chi(\omega)/(\chi(\omega) + 2)$. The presence of vibrational resonances contributes to $\chi(\omega)$, and therefore $\beta(\omega)$ depends on the vibrational resonances of the sample. In traditional linear near-field scattering, only the linear term $\chi^{(1)}(\omega)$ is considered. The presence of the image dipole in turn reinforces the field at the tip apex located at $2(r + d)$, leading to an increase of the local electric field due to the image dipole $\beta(\omega)P(\omega)/16\pi(r + d)^3$. The polarization of the induced dipole at the tip apex should be self-consistent and is expressed in Eq. (S2).

$$P(\omega) = \alpha \mathrm{E}(\omega) + \alpha \frac{\beta(\omega)\mathrm{P}(\omega)}{16\pi(r + d)^3} \qquad (S2)$$

The solution gives $P(\omega)$. $P(\omega)$ as expressed in Eq. (S3), as a function of tip radius r, tip-sample distance d, dielectric functions ϵ_t and $\epsilon(\omega)$ and external incident field $E(\omega)$.

$$P(\omega) = \alpha \left(1 - \frac{\alpha\beta(\omega)}{16\pi(r + d)^3}\right)^{-1} \mathrm{E}(\omega) \qquad (S3)$$

$P(\omega)$ plays a central role in describing the linear near-field scattering of a metallic tip above a

vibrationally resonant sample.

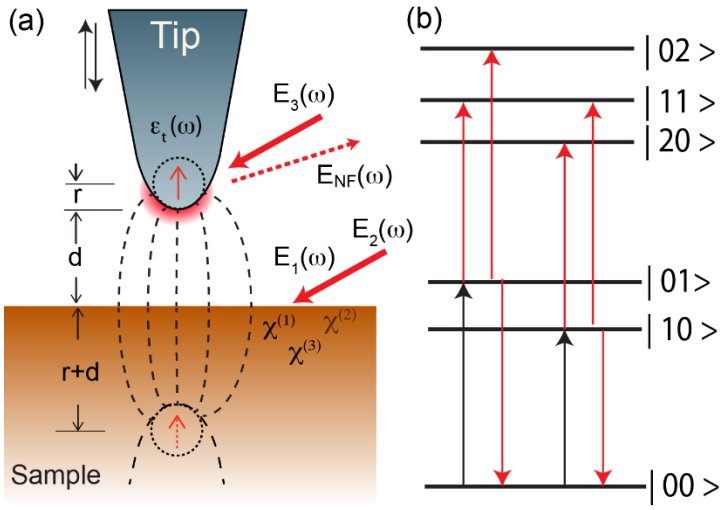

Figure S6. (a) Illustration of the image dipole model. (b) The vibrational level diagram of two coupled vibrational modes. The black arrows represent the transitions that are available to single field excitation. The red arrows represent the available transitions for the subsequent "probe" field.

Retrieving mode coupling information requires nonlinear interactions with additional infrared preparation fields in addition to the near-field scattering. Preparation fields interact with the sample to create the excited-state population and the superposition (coherence) of the two excited states, which last according to the de-population time or decoherence of the excited levels respectively. Both population and polarization at the excited vibrational levels affect the interaction of the probe field, making possible short-lived excitation pathways that are otherwise not allowed by a single beam linear measurement[8] (see Figure S6b). Taking a system with two vibrational resonances v_1 and v_2 as an example, the absorption process of a single electric field by molecular vibrational resonances corresponds to the generation of polarization between the ground state $|00>$ and singly excited $|01>$, or $|10>$ state. The ability to generate polarization at transition frequencies of v_1 and v_2 contributes to the imaginary (and real) part of the linear dielectric function $\epsilon(\omega)$ or the linear term of susceptibility $\chi^{(1)}$. The polarization between doubly excited state $|11>$ and ground state $|00>$ does not directly couple to a single electric field, therefore does not contribute to $\chi^{(1)}$ directly. The continuing excitation of a probe field, however, allows subsequent excitation from $|01>$ and $|10>$ to doubly excited states $|02>$, $|20>$ and $|11>$. With the presence of preceding preparation fields, such allowed excitations can be mathematically treated as an additional term to the dielectric function $\epsilon(\omega)$, previously defined in a linear fashion, to form an overall effective dielectric function with dependent on multiple fields. In the field of nonlinear spectroscopy, such a modification to linear response is more conveniently represented by the nonlinear susceptibility $\chi^{(n)}$ with $n \geq 2$.

In the context of near-field two-dimensional infrared spectroscopy, it is the third order susceptibility $\chi^{(3)}$ that explicitly describes the vibrational mode coupling.[9] The role of $\chi^{(2)}$ in near-field scattering will be discussed later. We introduce two preparation fields, $E_1(\omega_1)$ and $E_2(\omega_2)$, interacting with the sample before the near-field scattering of the third field, $E_3(\omega_3)$, as the probe field. If $E_1(\omega_1)$ and $E_2(\omega_2)$ come from the same light source

with $\omega_1 = \omega_2$, the specific $-\omega_1 + \omega_2 + \omega_3$ and $\omega_1 - \omega_2 + \omega_3$ terms in $\chi^{(3)}$ contribute to the polarization at frequency ω_3, which is the same frequency as the linear polarization generated by $E_3(\omega)$, alone through $\chi^{(1)}$.[10]

A comparison between the linear and nonlinear polarizations in the image dipole model provides understanding of the modification of the image dipole through $\chi^{(3)}$. In linear near-field scattering, the polarization of a sample with just a probe field is $P(\omega) = \chi^{(1)}(\omega{:}\,\omega_3)E_3(\omega_3)$. In near-field two-dimensional scattering, the polarization of the sample at the probe field frequency contains not only the linear term $P^{(1)}(\omega) = \chi^{(1)}(\omega{:}\,\omega_3)E_3(\omega_3)$, but also the third order term: $P^{(3)}(\omega) = \left[\chi^{(3)}(\omega{:}\,\omega_1, -\omega_2, \omega_3)E(\omega_1)E^*(\omega_2) + \chi^{(3)}(\omega{:}\,-\omega_1, \omega_2, \omega_3)E^*(\omega_1)E(\omega_2)\right]E(\omega_3)$. Using the definition of $\chi(\omega) = P(\omega)/E(\omega)$ and $P(\omega) = P^1(\omega) + P^{(3)}(\omega)$, the overall susceptibility at frequency ω is shown by Eq. (S4)

$$\chi(\omega) = \chi^{(1)}(\omega{:}\,\omega_3) + \chi^{(3)}(\omega{:}\,\omega_1, -\omega_2, \omega_3){:}\,E_1(\omega_1)E_2^*(\omega_2) + \chi^{(3)}(\omega{:}\,-\omega_1, \omega_2, \omega_3){:}\,E_1^*(\omega_1)E_2(\omega_2) \quad \text{(S4)}$$

For conciseness, the relevant $\chi^{(3)}$ terms are shorthanded as $\chi^{(3)}{:}\,E_1E_2$, and $\chi^{(1)}(\omega{:}\,\omega_3)$ as $\chi^{(1)}$ in the following section. Combined with Eq. (S3), the polarization of the tip dipole with near-field coupled image dipole is obtained in Eq. (S5)

$$P(\omega) = \left[\frac{1}{\alpha} - \frac{1}{u(r,d)}\left(1 - \frac{2}{2+\chi^{(1)}+\chi^{(3)}:E_1E_2}\right)\right]^{-1} E_3(\omega) \quad \text{(S5)}$$

Here, $u(r,d)$ is used to represent the distance dependent $16(r+d)^3$ term for conciseness. Eq. (S5) is the central equation that describes the source polarization of the near-field two-dimensional scattering signal, emitted from the metallic scanning probe tip above the resonant sample. We call it a rectified linear image dipole model for two-dimensional near-field scattering. The term $\left[\frac{1}{\alpha} - \frac{1}{u(r,d)}\left(1 - \frac{2}{2+\chi^{(1)}+\chi^{(3)}:E_1E_2}\right]^{-1}\right.$ is the polarizability of the tip and sample with $\chi^{(3)}$ contribution.

The emitted signal is $E_{NF} = bP(\omega)$, with b as a scaling factor representing the overall signal collection and detection coefficient.

The near-field signal $S(\omega)$ is proportional to the effective polarizability, expressed by Eq. (S6).

$$S(\omega) = b\left[\frac{1}{\alpha} - \frac{1}{u(r,d)}\left(1 - \frac{2}{2 + \chi^{(1)} + \chi^{(3)}: E_1 E_2}\right)\right]^{-1} E_3(\omega) \qquad (S6)$$

The experimentally measurable quantity $S(\omega)$ is now described by the right hand side of Eq. (S6), which describes the near-field scattering with nonlinear response $\chi^{(3)}$. It is linearly proportional to the tip-sample polarizability with the scaling factor *b*.

The nonlinear contribution to χ is typically small compared to the linear contribution. Therefore, we can make an approximation by treating the nonlinear response $\chi^{(3)}$ as a small perturbation to $\chi^{(1)}$ due to the presence of the pump field, and use the linear expansion $\Delta f(\chi) \approx \frac{df(\chi)}{d\chi}\Delta\chi$ of the right hand side of Eq. (S6) to find the relation between the near-field signal difference $\Delta S(\omega)$ and the third order susceptibility $\chi^{(3)}$ in Eq. (S7)

$$\Delta S(\omega) \approx 2b\left[u(r,d)\left(\frac{1}{\alpha}-\frac{1}{u(r,d)}+\frac{2}{u(r,d)(2+\chi^{(1)})}\right)^2\left(2+\chi^{(1)}\right)^2\right]\chi^{(3)}\!:E_1E_2 \qquad (S7)$$

where $\Delta S(\omega)$ is the signal difference between with and without the pump field. The signal difference is obtained with the doubly demodulated lock-in detection in our experiment. In Eq. (S7), the measureable near-field signal difference, $\Delta S(\omega)$, is linearly proportional to the third order nonlinear susceptibility with preparation fields, modified by a near-field envelope function preceding the $\chi^{(3)}$term in Eq. (S7). Eq. (S7) directly relates near-field measurable quantities, $\Delta S(\omega)$, to the component of the third order susceptibility, $\chi^{(3)}$, that carries mode coupling information. Therefore, it bridges scattering type near-field microscopy with two-color infrared spectroscopy. In correspondence to the main text, the pump field acts twice as E_1 and E_2.

We note that are special circumstances under which $\chi^{(2)}$ processes may contribute to the signal. In this case, Eq (S5) should be replaced with

$$P(\omega) = \left[\frac{1}{\alpha}-\frac{1}{u(r,d)}\left(1-\frac{2}{2+\chi^{(1)}+\chi^{(2)}E_1+\chi^{(3)}\!:{E_1}^2}\right)\right]^{-1}E_2(\omega) \qquad (S12)$$

where $u(r,d) = 16\,(r+d)^3$, E_1 and E_2 are the pump and probe field respectively. This results in

$$\Delta S(\omega) \approx 2b\left[u(r,d)\left(\frac{1}{\alpha}-\frac{1}{u(r,d)}+\frac{2}{u(r,d)(2+\chi^{(1)})}\right)^2\left(2+\chi^{(1)}\right)^2\right]^{-1}\left(\chi^{(2)}E_1 + \chi^{(3)}\!:E_1^2\right)$$

where $\Delta S(\omega)$ is the signal difference between with and without the pump field. A situation when the $\chi^{(2)}$ contribution may be significant includes resonant-enhanced sum-frequency or difference frequency generation.

---

[1] Golberg, D.; Mitome, M.; Bando, Y.; Tang, C.C.; Zhi , C.Y. Multi-walled boron nitride nanotubes composed of diverse cross-section and helix type shells. *Applied Physics A*, August **2007**, Volume 88, Issue 2, pp 347-352.

[2] Rokuta, E.; Hasegawa, Y.; Suzuki, K.; Gamou, Y.; Oshima, C. Phonon Dispersion of an Epitaxial Monolayer Film of Hexagonal Boron Nitride on Ni (111). *Phys. Rev. Lett.*, **1997**, 79, 4609.

[3] Wang, B.; List, J. Basic Optical Properties of The Photoelastic Modulator Part I: Useful Aperture and Acceptance Angle. *SPIE Proceedings*, vol 5888, **2005.**

[4] Jackson, J. D. *Classical Electrodynamics*, 3rd ed.; Wiley, **1998**.

[5] Knoll, B.; Keilmann, F. Enhanced dielectric contrast in scattering-type scanning near-field optical microscopy. *Optics Communications.* **2000**, 182, 321–328.

[6] Raschke, M. B.; Lienau, C. Apertureless near-field optical microscopy: Tip-sample coupling in elastic light scattering. *Applied Physics Letters*. **2003**, 83, 5089–5091.

[7] Cvitkovic, A.; Ocelic, N.; Hillenbrand, R. Analytical model for quantitative prediction of material contrasts in scattering-type near-field optical microscopy. *Optics Express.* **2007**, 15,8550–8565.

[8] Hamm, P.; Zanni, M. T. *Concepts and Methods of 2D Infrared Spectroscopy*. Cambridge University Press, **2011**.

[9] Mukamel, S. *Principles of Nonlinear Optical Spectroscopy*. Oxford Press, **1999**.

[10] We use the notation of w1-w2+w3 instead of k1-k2+k3, because the near-field is evanescent, leading to the imaginary propagating wave vector k.